1   An analog to digital converter creates nuclear localization pulses in yeast calcium signaling

2   Ian S Hsu, Bob Strome, Sergey Plotnikov, Alan M Moses

3   Department of Cell & Systems Biology

4   University of Toronto

5

6   Abstract:

7   Several examples of transcription factors that show stochastic, unsynchronized pulses of nuclear

8   localization have been described. Here we show that under constant calcium stress, nuclear

9   localization pulses of the transcription factor Crz1 follow stochastic variations in cytoplasmic

10   calcium concentration. We find that the size of the stochastic calcium pulses is positively

11   correlated with the number of subsequent Crz1 pulses. Based on our observations, we propose a

12   simple stochastic model of how the signaling pathway converts a constant external calcium

13   concentration into a digital number of Crz1 pulses in the nucleus, due to the time delay from

14   nuclear transport and the stochastic decoherence of individual Crz1 molecule dynamics. We find

15   support for several additional predictions of the model and conclude that stochastic input to

16   nuclear transport may produce digital responses to analog signals in other signaling systems.

17   Keywords: stochastic pulsing transcription factor, Crz1, time delay model, mathematical

18   modeling, calcineurin pathway

19   Introduction:

20   Cells transmit information through signaling pathways. Rather than simple "ON" or "OFF"

21   responses, several key pathways (p53, NF-κB, and others) are now appreciated to encode

22   information in the dynamics of the signaling response(1–9). Here we focus on the calcium

23   signaling pathway in yeast, which controls gene transcription through frequency modulation

24   (FM) of the transcription factor Crz1(9). In this system, the analog external calcium

25   concentration is converted into the frequency of digital pulses of nuclear localization (discrete

26   rapid rising and falling of nuclear concentration on the order a few minutes).

27   Mechanistic models of FM pulsatile transcription factors have relied on negative feedback

28   coupled with positive feedback(7,8,10,11) or delayed negative feedback(11,12). However,

29   whether there is a negative feedback loop in calcium signaling pathway that can generate Crz1

30   pulses is unclear (discussed further below). Furthermore, in each cell, during each Crz1 nuclear

31   localization pulse, approximately 500 Crz1 molecules are transported in and out of the nucleus in

32   a coordinated fashion(13), but these pulses are stochastic (and not synchronized between cells).

33   To our knowledge, no mechanistic model of this process has yet been proposed.

34   One possibility is that Crz1 nuclear localization pulses are connected to variation in cytoplasmic

35   calcium concentration ($[Ca^{2+}]_{cyt}$) since calcineurin is activated by calcium(14). Calcium pulses

36   have been observed in many cell types(15–19), but the connections between cytoplasmic calcium

37   concentration and Crz1 localization have not been analyzed in single cells. Mechanistic models

38   of Crz1 regulation through calcium signaling do not predict external calcium concentration

39   ($[Ca^{2+}]_{ext}$)-induced oscillation of $[Ca^{2+}]_{cyt}$(20). Further, although average Crz1 nuclear

40   localization increases when $[Ca^{2+}]_{ext}$ increases(9), $[Ca^{2+}]_{cyt}$ is known to be under tight

41   homeostatic control: the average $[Ca^{2+}]_{cyt}$ remains similar under a wide range of $[Ca^{2+}]_{ext}$(21,22).

42   Variation in $[Ca^{2+}]_{cyt}$ is unlikely to follow the frequency of Crz1 pulsatility, which increases

2

43   when $[Ca^{2+}]_{ext}$ increases(9). Thus, the relationship between calcium and Crz1 pulses remains

44   unclear.

45   In this study, we examined the connection between $[Ca^{2+}]_{cyt}$ and Crz1 pulsatile dynamics through

46   dual fluorescence time-lapse microscopy(23). We found that cytoplasmic calcium concentration

47   varies stochastically at the single cell level, showing pulses on the timescale of 10-100 seconds.

48   We observed overshoots of the calcium concentration, strongly implicating calcium channels in

49   these pulses. We found that Crz1 pulses tend to follow these calcium pulses, but that the

50   relationship is not simple: multiple Crz1 pulses may follow each calcium pulse, and the number

51   of Crz1 pulses depends on the size of the calcium pulse. We modulated calcium channel activity

52   and found much larger calcium pulses, which led to greater numbers of Crz1 pulses. To explain

53   how $[Ca^{2+}]_{cyt}$ affects Crz1 nuclear localization, we developed a stochastic model of Crz1 nuclear

54   localization and tested predictions in the experimental data. In general, stochastic pulses in

55   signaling dynamics may be generated by time-delayed responses to fluctuations in second

56   messenger concentration.

57   Results

58   *Calcium pulses are observed when yeast cells are under calcium stress*

59   In order to study the relationship between the dynamics of $[Ca^{2+}]_{cyt}$ and Crz1 nuclear

60   localization, we constructed a dual Crz1-Calcium reporter strain and measured dynamics using

61   time-lapse microscopy. We tagged Crz1 with the mCherry fluorescent protein in a strain with a

62   cytoplasmicly expressed calcium sensor GCaMP3(16), and recorded movies on a confocal

63   fluorescence microscope (see Methods). As in previous studies(9), we observed stochastic and

64   rapid increases and decreases of $[Ca^{2+}]_{cyt}$ when yeast are under calcium stress (Figure 1 A,

65 supplementary video 1). We noticed that these "calcium pulses" (defined by a threshold ratio

66 above background, see Methods) are followed by an overshoot of calcium concentration below

67 the resting level (average of 50 largest calcium local maxima in a representative time lapse

68 movie is shown in Figure 1B left panel), whose depth is positively correlated to the height of the

69 pulse (Figure 1B, right panel, $R^2 = 0.37$). This overshoot cannot fit an exponential curve and

70 suggests negative feedback on $[Ca^{2+}]_{cyt}$, which is consistent with the predictions of calcium

71 models constructed in previous studies of homeostasis[24,25].

72 *Quantification of calcium pulses and Crz1 pulses suggests an analog to digital converter*

73 Individual cell trajectories do not show a simple relationship between $[Ca^{2+}]_{cyt}$ and Crz1 nuclear

74 localization (Figure 1A), so we next sought to understand how Crz1 pulses (see Methods for

75 definition of Crz1 pulses) are affected by calcium pulses. We analyzed the distribution of the

76 time differences between a calcium pulse and following Crz1 pulse(s) (using so-called pulse-

77 triggered averaging[23]). The coherence of the first and second pulses suggested to us that one or

78 more Crz1 pulses follows a single calcium pulse (Figure 2A). We therefore compared the time

79 until the first Crz1 pulse within 10 minutes of a calcium pulse to the time until the first Crz1

80 pulse within 10 minutes from a randomly chosen cell that may or may not contain a calcium

81 pulse. Consistent with our hypothesis, we found that the time until the first Crz1 pulses after

82 calcium pulses shows reduced standard deviation (122.47 seconds vs. 161.25 seconds, F-test,

83 p<0.005, n = 168) and occurs sooner than observed in randomly chosen cells (83.01+-9.58

84 seconds vs. 210.62+-28.89 for random, two-tailed t-test, p $<10^{-15}$, n = 193). A similar range of

85 time differences is also observed in cross correlation analysis (supplementary figure 1).

86 Furthermore, the distributions of time differences disperse when the order of Crz1 pulses

87 increases (Figure 2A, e.g., 122.47 seconds, n = 81 for first pulses vs. 181.66 seconds, n = 45 for

88   second pulses, F-test, p<0.005), suggesting that the effect of the calcium pulse on Crz1 dynamics

89   decreases over time. These results suggest that one calcium pulse can lead to multiple Crz1

90   pulses.

91   We sought to identify factors that determine the number of Crz1 pulses that follow each calcium

92   pulse. We found that the number of Crz1 pulses after a calcium pulse is positively correlated to

93   the height of that calcium pulse (Figure 2B, generalized linear model regression with Poisson

94   distribution, slope = 0.16+-0.10). To test whether a calcium pulse causes Crz1 pulses, we tested

95   whether there is a correlation between calcium pulse height and the number of Crz1 pulses

96   before a calcium pulse. If an (unmeasured) third factor affects both the height of a calcium pulse

97   and the number of the Crz1 pulses in a cell, we expect more Crz1 pulses both before and after

98   large calcium pulses. We found that the number before is not correlated with calcium pulse size

99   (slope = -0.10+-0.13, generalized linear model regression with Poisson distribution). This result

100   is consistent with the idea that calcium pulses can cause more than one Crz1 pulse, and suggests

101   that calcium pulse heights are converted into digital numbers of Crz1 pulses.

102   *Artificially increased calcium pulse height supports the analog to digital converter model*

103   The hypothesis of an analog to digital converter between calcium pulse height and Crz1 pulse

104   number predicts that the average number of Crz1 pulses following calcium pulses could be made

105   larger by artificially inducing larger calcium pulses. To test this prediction, we treated cells with

106   nifedipine (See Methods). By doing so, we reliably induced synchronized calcium pulses

107   (supplementary video 2) that were on average twice as large as the stochastic pulses observed at

108   steady state in 0.2M calcium treatment alone (Figure 3A, compared to Figure 1B). The majority

109   of these large calcium pulses are followed by at least 4 Crz1 pulses that disperse over time

110   (Figure 3B). As predicted by the model, the number of Crz1 pulses after a calcium pulse is

5

111 positively correlated to calcium pulse height, and the range is larger than untreated range (Figure

112 3C, compared to Figure 2B, generalized linear model regression with Poisson distribution, slope

113 = 0.37+-0.11). In individual cells, nuclear Crz1 now clearly appears to oscillate while no

114 oscillations are observed in cytoplasmic calcium concentration (supplementary figure 2). These

115 results confirm that single calcium pulses are followed by multiple Crz1 pulses, and support the

116 idea that an analog-to-digital converter in the calmodulin/calcineurin signaling pathway converts

117 calcium pulse height into Crz1 pulse number.

118 *A simple time delay model can reproduce the properties of Crz1 pulses after a calcium pulse*

119 To explain the mechanism of the analog to digital converter, we considered a two-step process in

120 single cells (Figure 4A). The first step is that external calcium concentration leads to cytoplasmic

121 calcium pulses (4A, blue trace) through stochastic channel opening, and the second step is that a

122 calcium pulse leads to nuclear Crz1 pulses (4A, red trace) through the calcineurin pathway.

123 A negative feedback loop in the calcineurin pathway could lead to oscillation of calcineurin

124 activity and drive Crz1 pulses, but we decided not to include one in our model for two reasons.

125 First, the known negative feedback loop in the calcineurin pathway through Rcn1 does not

126 appear to affect Crz1 pulsatility. Rcn1 is an inhibitor of calcineurin that is degraded when

127 phosphorylated and is dephosphorylated by activated calcineurin (26,27), thus leading to

128 negative feedback. However, the negative feedback loop is thought to be controlled by the

129 protein abundance of Rcn1, as phosphorylation does not prevent Rcn1's inhibition of

130 calcineurin(26). Since Crz1 pulsatility occurs when protein synthesis is inhibited by

131 cycloheximide (supplementary figure 3) we consider it unlikely that Rcn1 provides negative

132 feedback through changes in protein abundance. Second, models with feedback mechanisms

6

133   seem incompatible with the observation that the frequency but not the amplitude of Crz1 pulses

134   increases when the affinity of calcineurin docking site on Crz1 is enhanced(9). This is opposite

135   to the expectation if Crz1 nucleocytoplasmic transition were driven by a feedback mechanism.

136   Therefore, we worked toward models that do not include a feedback mechanism.

137   Previously, Crz1 nuclear localization dynamics were explained with a conformational switch

138   model(22). This model assumes that the large number of phosphorylation sites on Crz1 leads to a

139   sigmoid function relating calcineurin activity to Crz1 nuclear localization, so when calcineurin

140   activity swings above and below a threshold, Crz1 sensitively reads out the perturbation in

141   calcineurin activity and switches fully nuclear or cytoplasmic (22,28). This model would predict

142   that calcium concentration crosses a threshold before each Crz1 pulse, and pulses stop once

143   calcium oscillations decay below the threshold. However, calcium is not observed to pass a

144   threshold before each Crz1 pulse in our data (supplementary figure 2D for examples).

145   We therefore considered another single cell model. Inspired by the observations on the

146   population level that Crz1 pulses tend to occur within 100 seconds after calcium pulses and then

147   disperse over time, and that larger calcium pulses lead to more Crz1 pulses, we constructed a

148   discrete-time stochastic model that explains single cell Crz1 nuclear localization based on time

149   delays during nuclear import and export with variation among Crz1 molecules. Time delay

150   models have been constructed through different approaches, including deterministic and

151   stochastic delay differential equations with a fixed or variable delay periods(12,29–31). We used

152   a discrete-time Markov chain because it is simple to simulate trajectories. In the model, Crz1

153   molecules transit between the nucleus and the cytoplasm in a coordinated manner (show pulsing

154   dynamics on average) only when calcineurin activity is very high due to a recent calcium pulse.

7

155 As calcineurin activity slowly returns to its basal level, the coordinated transport of 500 Crz1

156 molecules in a single cell decoheres.

157 We model Crz1 nuclear signal by aggregating the states of individual Crz1 molecules after an

158 increase in cytoplasmic calcium concentration of a single cell. As the input to the model, we

159 provide calcium concentration, Ca, as a function of time, t, which can be obtained from

160 experimental data (using GCaMP reporter fluorescence as a proxy).

161 We assume that calcineurin activity at time t, $Cn(t)$, has an activation rate proportional to

162 calcium concentration and a constant rate of decay. The discrete time dynamics of $Cn(t)$ is

163 described by

164 $\Delta Cn \equiv Cn(t+1) - Cn(\mathrm{t}) = \left(Cn_{base} - Cn(t)\right) D + \max[0, Ca(t)] A,$

165 where Cn_{base} is the basal activity of calcineurin, D is the decay rate of calcineurin activity, and

166 A is the activation rate by cytoplasmic calcium. Although calcium concentration can never be

167 negative, our GCaMP reporter data is normalized such that baseline fluorescence level is defined

168 as 0. When calcium pulses overshoot, we obtain negative values, and hence include

169 $\max[0, Ca(t)]$ in the equation above. The probability of a Crz1 molecule being imported is $Cn(t)$

170 multiplied by the probability of dephosphorylation by an active calcineurin molecule (see

171 Methods for details). Thus, when calcineurin activity increases, the probability of a Crz1

172 molecular being imported increases.

173 Once a Crz1 molecule is imported into the nucleus, it returns to the cytoplasm after it is

174 phosphorylated in the nucleus, which we assume occurs at a constant rate. These chemical

175 reactions can be formulated using a standard biochemical rate approach as

$$X_C \overset{a}{\Rightarrow} X_N, \qquad X_N \overset{b}{\Rightarrow} X_C,$$

8

176   where X_C and X_N are cytoplasmic and nuclear Crz1 molecules, respectively, and a and b are the

177   rates of delayed transports (denoted as thick arrows). In our Markov chain framework, we

178   assume that transports are multistage, so the delay time follows a Gamma distribution with the

179   two parameters related to the number of states and the transition probability (see Supplementary

180   text for details).

181   This model can qualitatively reproduce Crz1 pulses after a calcium pulse (Figure 4B). The

182   number of Crz1 pulses after a calcium pulse is positively correlated to the height of that calcium

183   pulse (Figure 4C, generalized linear model regression with Poisson distribution, slope = 0.29+-

184   0.13), while the number of that before a calcium pulse is not (slope = 0.02+-0.16).

185   *Other predictions of the model are found in the experimental data*

186   The time delay model also predicts other properties of Crz1 pulsatility. A first prediction is that

187   the periodicity of a Crz1 trajectory is correlated with calcium pulse size, such that a Crz1

188   trajectory after a larger calcium pulse keeps oscillating longer. To test this prediction, we

189   quantified the periodicity of Crz1 dynamics after the largest calcium pulse of each cell using a

190   Gaussian Process model (see Methods), which computes the log-likelihood ratio (LLR)

191   comparing a periodic to an aperiodic kernel. The LLR of post-calcium-pulse trajectories is

192   correlated to the height of calcium pulses (Figure 5A). Calcium pulses larger than 0.11 show

193   LLR significantly larger than that of the rest (two tailed t-test, sample sizes are 92 and 95, $p < 10^{-5}$

194   ), which means larger calcium pulses lead to Crz1 dynamics that can be better described by a

195   periodic Gaussian process. As a control, we also computed the LLR for pre-calcium-pulse

196   trajectories, and found that the pre-calcium-pulse trajectories of for calcium pulse height above

197   0.11 are not statistically more periodic (p >0.1). Periodic dynamics after large calcium pulses

198   would also be predicted by conformational switch model, where, after a larger calcium pulse,

199   calcium oscillates longer and has more peaks crossing a threshold to trigger Crz1 pulse

200   (supplementary figure 4).

201   Additional predictions of the time delay model are that, after a calcium pulse that is followed by

202   at least two Crz1 pulses, the second Crz1 pulse is shorter and wider than the first Crz1 pulse

203   because the coordinated transport of Crz1 molecules disperses across time. Although both the

204   conformational switch model and the time delay model predict shorter second Crz1 pulses, the

205   conformational switch model would predict a narrower second Crz1 pulse as the calcium

206   oscillations decay (Figure 5C). To test these predictions, we identified the calcium pulses that are

207   followed by two Crz1 pulses, and fit them to a "logistic pulse model" (Figure 5B, median $R^2 =$

208   0.85, mean $R^2 = 0.79$, See Methods) to estimate pulse height and narrowness. We found that the

209   height of the second pulse is significantly smaller (Figure 5D, paired t-test, $p < 0.005$, n =42),

210   and that the mean narrowness of the second pulses is significantly smaller than that of the first

211   pulses (Figure 5D, paired t-test, $p < 10^{-8}$, n = 42), supporting the time delay model to the

212   exclusion of the conformational switch model.

213   Thus, the data support three additional predictions of a simple stochastic model of Crz1 nuclear

214   import and export. Together with the explanation of the analog to digital converter, our results

215   support the idea that coordination of Crz1 localization (and thus pulsatility) is the result of a

216   time-delay in nuclear import and export (see Discussion).

217   Discussion

218   Our results show that $[Ca^{2+}]_{cyt}$ is linked to Crz1 pulsatility through an analog to digital

219   conversion: larger calcium pulses lead to more Crz1 pulses. Through this model, we can explain

10

220   Crz1 pulses found after calcium pulses and provide a possible link between irregular Ca^{2+}

221   oscillation and transcription(17). However, in our cells, Crz1 fluctuations are also found without

222   preceding calcium pulses. These Crz1 fluctuations are aperiodic and do not show correlations

223   between number of pulses and calcium size. We recorded movies at four different $[Ca^{2+}]_{ext}$, and

224   found that, although the frequency of calcium pulses is correlated with external calcium

225   concentration, the increase in calcium pulsing frequency is not comparable to the increase in

226   Crz1 pulsing frequency, and the average size of calcium pulses does not increase significantly.

227   Therefore, our model cannot fully explain the calcium concentration dependence of Crz1

228   fluctuations. However, cross-correlation analysis shows that these Crz1 dynamics have only a

229   small correlation with $[Ca^{2+}]_{cyt}$ dynamics (supplementary figure 1). We suggest that other

230   intrinsic environmental fluctuations that affect Crz1 localization, such as light-(32), osmotic

231   pressure-(33), or glucose-(34,35) induced Crz1 regulation might be involved in producing these

232   fluctuations.

233   One of the interesting properties of pulsatile dynamics is that the pulses in individual cells are

234   not synchronized, despite cells experiencing the same environmental stress(36). The analog-

235   digital converter model explains this aspect of Crz1 pulsatility by arguing that the $[Ca^{2+}]_{cyt}$

236   among individual cells at a given time point is stochastic, perhaps due to spontaneous Ca^{2+}

237   transients(37). This model predicts that, if calcium pulses among cells could be synchronized in

238   time, then Crz1 pulsatility should be synchronized immediately after, and that this induced

239   synchrony would gradually decay. Consistent with this, in our nifedipine treated cells where

240   large calcium pulses were induced in every cell immediately after calcium was added to the

241   media, the Crz1 pulses following these synchronized calcium pulses are also synchronized, and

242   this synchrony decays with time (Figure 3B). However, by simulating Crz1 dynamic many times

243   with identical parameter values (Table 1), we found that our stochastic time delay model does

244   not predict this loss of synchrony at the population level. This suggests that additional sources of

245   cell-to-cell variability are likely missing from the stochastic time delay model.

246   Nevertheless, our stochastic time delay model has several advantages over a conformational

247   switch model that assumes Crz1 nuclear localization sensitively reads out $[Ca^{2+}]_{cyt}$ when $[Ca^{2+}]_{cyt}$

248   passes through a threshold(22). Once a damped calcium oscillation is present, the conformational

249   switch model can generate Crz1 pulses as a readout of $[Ca^{2+}]_{cyt}$ passing through a threshold

250   (supplementary figure 4). Although we do not observe calcium oscillations passing a threshold in

251   our movies, it is possible that our calcium sensor is not sensitive enough to distinguish these

252   dynamics from background noise. Both our model and the conformational switch model require

253   no negative feedback in the calmodulin/calcineurin signaling pathway. However, our model

254   predicts the width of the second Crz1 pulse to be wider than the first, while the conformational

255   switch model predicts the opposite: a narrower second Crz1 pulse because it is reading out a

256   smaller fluctuation in $[Ca^{2+}]_{cyt}$. The comparison of pulse widths (Figure 5D) supports the time

257   delay model. We also note that the stochastic model is simpler (fewer parameters needed to

258   generate pulses and no assumption a sensitive threshold), and can directly explain the

259   coordination of the subcellular localization of the ~500 Crz1 molecules in the cell through time-

260   delay in nuclear transport.

261   One crucial assumption in our model for the coordination among Crz1 molecules is the

262   deactivation rate of calcineurin. Previous studies show that calcineurin has a deactivation rate *in*

263   *vitro* of 0.08 fold change per minute while both calcium ions and calmodulin are presented, and

264   has an even slower deactivation rate when either of them is not presented(38–40). The

265   deactivation rate is slow enough to maintain the synchronous translocation of each Crz1

266 molecule in our model, which only requires calcineurin to return to baseline activity around 5

267 minutes after a calcium pulse, a length of time that has been reported *in vitro*(38–40). A

268 conclusive test of our model would be a mutation in calcineurin that solely affects the

269 deactivation rate, but no such mutant is available to our knowledge.

270 Previous work on Crz1 pulsatility suggested that Crz1 pulses are actively generated rather than

271 passively reading out the fluctuation in $[Ca^{2+}]_{cyt}$(9). If our model is correct, then it suggests a

272 third possibility: individual Crz1 molecules read out $[Ca^{2+}]_{cyt}$ with a time delay. This possibility

273 can explain the observation that higher affinity of calcineurin docking site on Crz1 leads to

274 higher pulsing frequency(9), because higher affinity allows Crz1 to be dephosphorylated by a

275 lower fraction of activated calcineurin and, therefore, oscillate longer after a calcium pulse. The

276 time delay is assumed to be created by the transport between cytoplasm and nucleus, which

277 because it requires a complicated series of steps, leads to a transport rate in the order of

278 minutes(41). This model can be generalized to relocalization of other pulsatile transcription

279 factors and macromolecules that have dynamics on the order of minutes, and can explain how

280 signals that are short and fluctuating are converted into the frequency of pulses without a

281 negative feedback loop.

282

283 Materials and methods

284 *Yeast cell strain and growth conditions*

285 BY4741 was used to construct the dual Crz1-Calcium reporter strain. Plasmids expressing

286 GCaMP3 calcium reporter were constructed using Gibson assembly protocol(42) and gel

287   purification. The calcium reporter gene was assembled between the promoter of ribosomal

288   protein L39, RPL39, and the ADH1 terminator. pRPL39-GCaMP3-tADH1 was integrated at the

289   *HO* locus using a selectable marker (LEU2) and confirmed by Sanger sequencing. Four

290   replicates were performed and all showed expected GCaMP3 expression(15,16). To tag Crz1

291   with mCherry at the C terminus, genomic integration of pCrz1-ymCherry was done at the *CRZ1*

292   locus using a selectable marker (URA3) and confirmed by PCR. All transformations were

293   performed using the standard lithium acetate procedure(43).

294   All the time-lapse imaging experiments were started when cells were in log-phase (4 hours after

295   being diluted from overnight liquid culture). Cells were grown in synthetic complete (SC) media

296   lacking leucine and uracil to maintain section of markers. Carbon source was 2% glucose. For

297   artificially increased calcium pulse experiments, 200μm Nifedipine were added during the 4 hour

298   inoculation.

299   *Spinning-disk Confocal Microscopy and image analysis*

300   Nikon CSU-X1 was utilized for time-lapse imaging at room temperature (22° C). For GCaMP3,

301   488 nm laser was applied with time resolutions of 6 sec/frame, exposure time of 100 msec, and

302   25% laser intensity; for mCherry, 561 nm laser was applied with time resolution 30 sec/frame,

303   exposure time of 700 msec, and 50% laser intensity. Bright field images with out-of-focus black

304   cell edge were acquired every minute for cell segmentation and tracking.

305   Cells were attached to glass-bottom dishes with 0.1 mg/ml Concanavalin-A as a binding agent

306   using a standard protocol(44,45). For each experiment, a time-lapse image series without

307   calcium stress induction was recorded as a negative control. At the beginning of each time-lapse

308   image series, an area of the dish that had not been exposed to laser was recorded in order to

14

309   avoid blue light stress, which is known to induce Crz1 nuclear localization(32). Calcium chloride

310   solution was added to the dish to a final concentration of 0.2M through a syringe within 20

311   seconds. To record the dynamics during steady state, time-lapse movies of 30 min or 1 hour were

312   recorded after more than 1 hour of calcium stress induction for two to four time-lapse movies in

313   each experiment. 27 replicates of time-lapse movies (18 hours in total) were recorded. Every

314   analysis was done in both 1 hour and 30 minute time-lapse experiments.

315   Segmentation was automatically performed by identifying the area within cell edge through

316   MATLAB Image Segmentation Toolbox, and cell tracking was performed by identifying 90%

317   overlapping cell areas between two time frames. Mis-segmented and mis-stracked objects were

318   manually removed. 23-87 cells were identified in each time-lapse movie. Single cell

319   photobleaching correction was conducted after single cell reporter intensities were quantified

320   (see below) using bi-exponential regression(46): for GCaMP3 intensity, correction was

321   performed according to baseline intensity; for Crz1 expected nuclear signal, correction was

322   performed according to Crz1 expected cytoplasmic signal. Baseline was normalized to 0 after

323   photobleaching correction.

324   *Osmotic shock reduction*

325   Crz1 localizes into the nucleus for 10 to 15 minutes after an osmotic shock (33). In the

326   experiments where we artificially increased calcium pulses (nifedipine treatment), the effect

327   from osmotic shock was undesirable because the calcium pulses occur immediately after addition

328   of calcium. Change in osmotic pressure due to 0.2M calcium chloride is around 3.4 Pa, so prior

329   to the experiment, sodium chloride solution was added (to reach 0.4M) to increase osmotic

330   pressure to 6.1 Pa. When calcium chloride solution was added (so final concentrations of both

15

331   sodium chloride and calcium chloride were 0.2M), the final osmotic pressure was now around

332   6.5 Pa, reducing the change in osmotic pressure before and after addition of calcium to around

333   0.5 Pa.

334   *Reporter intensity quantification*

335   GCaMP3 intensity for each time point was estimated as average pixel intensity for all pixels in

336   the cell.

337   Nuclear localization for each time point was quantified by fitting a mixture of a Gaussian

338   distribution and a uniform distribution, and the parameters of distributions were estimated using

339   expectation-maximization on the pixel data from each cell (see supplementary text for more

340   details and derivation of the algorithm).

341   *Peak finding, pulse analyses and periodicity*

342   Local maxima/minima were identified with Matlab function findpeaks. To smooth fluctuations

343   shorter than 4 time points, Savitzky-Golay filtering was applied on each trajectory before

344   defining the Crz1 pulse threshold, identifying Crz1 pulses, and quantifying calcium overshoot

345   depth

346   To define the threshold for pulses, every local maximum in all cells growing in standard liquid

347   culture (no additional calcium) was identified with a minimum distance of 60 seconds.

348   Thresholds were then chosen to filter out most of the background noise: we chose the top 0.5%

349   of the peak height (0.09) for calcium pulses, and the top 5% of both the peak height (0.30) and

350   prominence (0.15) for Crz1 pulses.

351 For the analysis of the relationship between calcium pulse height and number of Crz1 pulses, the

352 Crz1 pulses following a calcium pulse were counted until the next calcium pulse or the end of

353 the time series, and the Crz1 pulses before a calcium pulse were counted until the previous

354 calcium pulse or the beginning of the time series.

355 For every cell that has its largest calcium pulse after 5 minutes from the beginning or before 5

356 minutes from the end of the time-lapse experiments, its Crz1 trajectory was separated into pre-

357 calcium-pulse and post-calcium-pulse trajectories. Each part was quantified if a trajectory prefers

358 an aperiodic Gaussian process model or a periodic Gaussian process model with log likelihood

359 ratio (LLR) using established method and MATLAB scripts(47).

360 *Logistic pulse fitting*

361 A least squares method is developed to quantify Crz1 pulse height and width based on the

362 analytic solution of logistic curve (see supplementary text for more details and derivation).

363 Acknowledgements

369 Conflict of interest

370   The authors of this manuscript do not have affiliation with or involvement in any organization or

371   entity with any financial interest or non-financial interest in the subject matter or materials

372   discussed in this manuscript.

373   Author contributions

374   I. S. H. performed the experiments. B. S. and S. P. provided experimental training and support. I.

375   S. H. and A. M. developed the computational models. A. M. supervised the project. I. S. H. and

376   A. M. wrote the paper.

377   References

378   1.   Purvis JE, Karhohs KW, Mock C, Batchelor E, Loewer A, Lahav G. p53 dynamics control
379   cell fate. Science. 2012 Jun 15;336(6087):1440–4.

380   2.   Ashall L, Horton CA, Nelson DE, Paszek P, Harper CV, Sillitoe K, et al. Pulsatile
381   stimulation determines timing and specificity of NF-kappaB-dependent transcription.
382   Science. 2009 Apr 10;324(5924):242–6.

383   3.   Hansen AS, O'Shea EK. Limits on information transduction through amplitude and
384   frequency regulation of transcription factor activity. eLife. 2015 May 18;4:e06559.

385   4.   Hansen AS, O'Shea EK. Encoding four gene expression programs in the activation
386   dynamics of a single transcription factor. Curr Biol CB. 2016 Apr 4;26(7):R269-271.

387   5.   Levine JH, Lin Y, Elowitz MB. Functional roles of pulsing in genetic circuits. Science.
388   2013 Dec 6;342(6163):1193–200.

389   6.   Nandagopal N, Santat LA, LeBon L, Sprinzak D, Bronner ME, Elowitz MB. Dynamic
390   Ligand Discrimination in the Notch Signaling Pathway. Cell. 2018 Feb 8;172(4):869-
391   880.e19.

392   7.   Albeck JG, Mills GB, Brugge JS. Frequency-modulated pulses of ERK activity transmit
393   quantitative proliferation signals. Mol Cell. 2013 Jan 24;49(2):249–61.

394   8.   Locke JCW, Young JW, Fontes M, Hernández Jiménez MJ, Elowitz MB. Stochastic pulse
395   regulation in bacterial stress response. Science. 2011 Oct 21;334(6054):366–9.

396   9.   Cai L, Dalal CK, Elowitz MB. Frequency-modulated nuclear localization bursts coordinate
397   gene regulation. Nature. 2008 Sep 25;455(7212):485–90.

10. Jiang Y, AkhavanAghdam Z, Tsimring LS, Hao N. Coupled feedback loops control the stimulus-dependent dynamics of the yeast transcription factor Msn2. J Biol Chem. 2017 28;292(30):12366–72.

11. Geva-Zatorsky N, Rosenfeld N, Itzkovitz S, Milo R, Sigal A, Dekel E, et al. Oscillations and variability in the p53 system. Mol Syst Biol. 2006;2:2006.0033.

12. Longo DM, Selimkhanov J, Kearns JD, Hasty J, Hoffmann A, Tsimring LS. Dual delayed feedback provides sensitivity and robustness to the NF-κB signaling module. PLoS Comput Biol. 2013;9(6):e1003112.

13. Kulak NA, Pichler G, Paron I, Nagaraj N, Mann M. Minimal, encapsulated proteomic-sample processing applied to copy-number estimation in eukaryotic cells. Nat Methods. 2014 Mar;11(3):319–24.

14. Cyert MS. Calcineurin signaling in Saccharomyces cerevisiae: how yeast go crazy in response to stress. Biochem Biophys Res Commun. 2003 Nov 28;311(4):1143–50.

15. Carbó N, Tarkowski N, Ipiña EP, Dawson SP, Aguilar PS. Sexual pheromone modulates the frequency of cytosolic Ca2+bursts inSaccharomyces cerevisiae. Mol Biol Cell. 2017 Feb 15;28(4):501–10.

16. Tian L, Hires SA, Mao T, Huber D, Chiappe ME, Chalasani SH, et al. Imaging neural activity in worms, flies and mice with improved GCaMP calcium indicators. Nat Methods. 2009 Dec;6(12):875–81.

17. Song S, Li J, Zhu L, Cai L, Xu Q, Ling C, et al. Irregular Ca(2+) oscillations regulate transcription via cumulative spike duration and spike amplitude. J Biol Chem. 2012 Nov 23;287(48):40246–55.

18. Sneyd J, Han JM, Wang L, Chen J, Yang X, Tanimura A, et al. On the dynamical structure of calcium oscillations. Proc Natl Acad Sci. 2017 Feb 14;114(7):1456–61.

19. Tsien RW, Tsien RY. Calcium channels, stores, and oscillations. Annu Rev Cell Biol. 1990;6:715–60.

20. Cui J, Kaandorp JA, Ositelu OO, Beaudry V, Knight A, Nanfack YF, et al. Simulating calcium influx and free calcium concentrations in yeast. Cell Calcium. 2009 Feb;45(2):123–32.

21. Miseta A, Fu L, Kellermayer R, Buckley J, Bedwell DM. The Golgi apparatus plays a significant role in the maintenance of Ca2+ homeostasis in the vps33Delta vacuolar biogenesis mutant of Saccharomyces cerevisiae. J Biol Chem. 1999 Feb 26;274(9):5939–47.

22. Cui J, Kaandorp JA. Mathematical modeling of calcium homeostasis in yeast cells. Cell Calcium. 2006 Apr;39(4):337–48.

23. Lin Y, Sohn CH, Dalal CK, Cai L, Elowitz MB. Combinatorial gene regulation by modulation of relative pulse timing. Nature. 2015 Nov 5;527(7576):54–8.

24. Ni XY, Drengstig T, Ruoff P. The control of the controller: molecular mechanisms for robust perfect adaptation and temperature compensation. Biophys J. 2009 Sep 2;97(5):1244–53.

25. Thorsen K, Agafonov O, Selstø CH, Jolma IW, Ni XY, Drengstig T, et al. Robust concentration and frequency control in oscillatory homeostats. PloS One. 2014;9(9):e107766.

26. Kishi T, Ikeda A, Nagao R, Koyama N. The SCFCdc4 ubiquitin ligase regulates calcineurin signaling through degradation of phosphorylated Rcn1, an inhibitor of calcineurin. Proc Natl Acad Sci. 2007 Oct 30;104(44):17418–23.

27. Rodríguez A, Roy J, Martínez-Martínez S, López-Maderuelo MD, Niño-Moreno P, Ortí L, et al. A conserved docking surface on calcineurin mediates interaction with substrates and immunosuppressants. Mol Cell. 2009 Mar 13;33(5):616–26.

28. Salazar C, Höfer T. Allosteric regulation of the transcription factor NFAT1 by multiple phosphorylation sites: a mathematical analysis. J Mol Biol. 2003 Mar 14;327(1):31–45.

29. Bratsun D, Volfson D, Tsimring LS, Hasty J. Delay-induced stochastic oscillations in gene regulation. Proc Natl Acad Sci U S A. 2005 Oct 11;102(41):14593–8.

30. Mittler JE, Sulzer B, Neumann AU, Perelson AS. Influence of delayed viral production on viral dynamics in HIV-1 infected patients. Math Biosci. 1998 Sep;152(2):143–63.

31. Galla T. Intrinsic fluctuations in stochastic delay systems: theoretical description and application to a simple model of gene regulation. Phys Rev E Stat Nonlin Soft Matter Phys. 2009 Aug;80(2 Pt 1):021909.

32. Bodvard K, Jörhov A, Blomberg A, Molin M, Käll M. The yeast transcription factor Crz1 is activated by light in a Ca2+/calcineurin-dependent and PKA-independent manner. PloS One. 2013;8(1):e53404.

33. Denis V, Cyert MS. Internal Ca(2+) release in yeast is triggered by hypertonic shock and mediated by a TRP channel homologue. J Cell Biol. 2002 Jan 7;156(1):29–34.

34. Bouillet LEM, Cardoso AS, Perovano E, Pereira RR, Ribeiro EMC, Trópia MJM, et al. The involvement of calcium carriers and of the vacuole in the glucose-induced calcium signaling and activation of the plasma membrane H(+)-ATPase in Saccharomyces cerevisiae cells. Cell Calcium. 2012 Jan;51(1):72–81.

35. D'hooge P, Coun C, Van Eyck V, Faes L, Ghillebert R, Mariën L, et al. Ca(2+) homeostasis in the budding yeast Saccharomyces cerevisiae: Impact of ER/Golgi Ca(2+) storage. Cell Calcium. 2015 Aug;58(2):226–35.

468   36.   Dalal CK, Cai L, Lin Y, Rahbar K, Elowitz MB. Pulsatile dynamics in the yeast proteome.
469   Curr Biol CB. 2014 Sep 22;24(18):2189–94.

470   37.   Baker SA, Drumm BT, Saur D, Hennig GW, Ward SM, Sanders KM. Spontaneous Ca(2+)
471   transients in interstitial cells of Cajal located within the deep muscular plexus of the murine
472   small intestine. J Physiol. 2016 15;594(12):3317–38.

473   38.   Kincaid RL, Martensen TM, Vaughan M. Modulation of calcineurin phosphotyrosyl protein
474   phosphatase activity by calmodulin and protease treatment. Biochem Biophys Res
475   Commun. 1986 Oct 15;140(1):320–8.

476   39.   Pallen CJ, Wang JH. Stoichiometry and dynamic interaction of metal ion activators with
477   calcineurin phosphatase. J Biol Chem. 1986 Dec 5;261(34):16115–20.

478   40.   King MM, Huang CY. The calmodulin-dependent activation and deactivation of the
479   phosphoprotein phosphatase, calcineurin, and the effect of nucleotides, pyrophosphate, and
480   divalent metal ions. Identification of calcineurin as a Zn and Fe metalloenzyme. J Biol
481   Chem. 1984 Jul 25;259(14):8847–56.

482   41.   Ribbeck K, Görlich D. Kinetic analysis of translocation through nuclear pore complexes.
483   EMBO J. 2001 Mar 15;20(6):1320–30.

484   42.   Gibson DG. Enzymatic assembly of overlapping DNA fragments. Methods Enzymol.
485   2011;498:349–61.

486   43.   Schiestl RH, Gietz RD. High efficiency transformation of intact yeast cells using single
487   stranded nucleic acids as a carrier. Curr Genet. 1989 Dec;16(5–6):339–46.

488   44.   Pemberton LF. Preparation of yeast cells for live-cell imaging and indirect
489   immunofluorescence. Methods Mol Biol Clifton NJ. 2014;1205:79–90.

490   45.   Zarin T, Tsai CN, Nguyen Ba AN, Moses AM. Selection maintains signaling function of a
491   highly diverged intrinsically disordered region. Proc Natl Acad Sci U S A. 2017 Feb
492   21;114(8):E1450–9.

493   46.   Vicente NB, Zamboni JED, Adur JF, Paravani EV, Casco VH. Photobleaching correction in
494   fluorescence microscopy images. J Phys Conf Ser. 2007;90(1):012068.

495   47.   Phillips NE, Manning C, Papalopulu N, Rattray M. Identifying stochastic oscillations in
496   single-cell live imaging time series using Gaussian processes. PLoS Comput Biol. 2017
497   May;13(5):e1005479.

498

499

500   Figure legends:
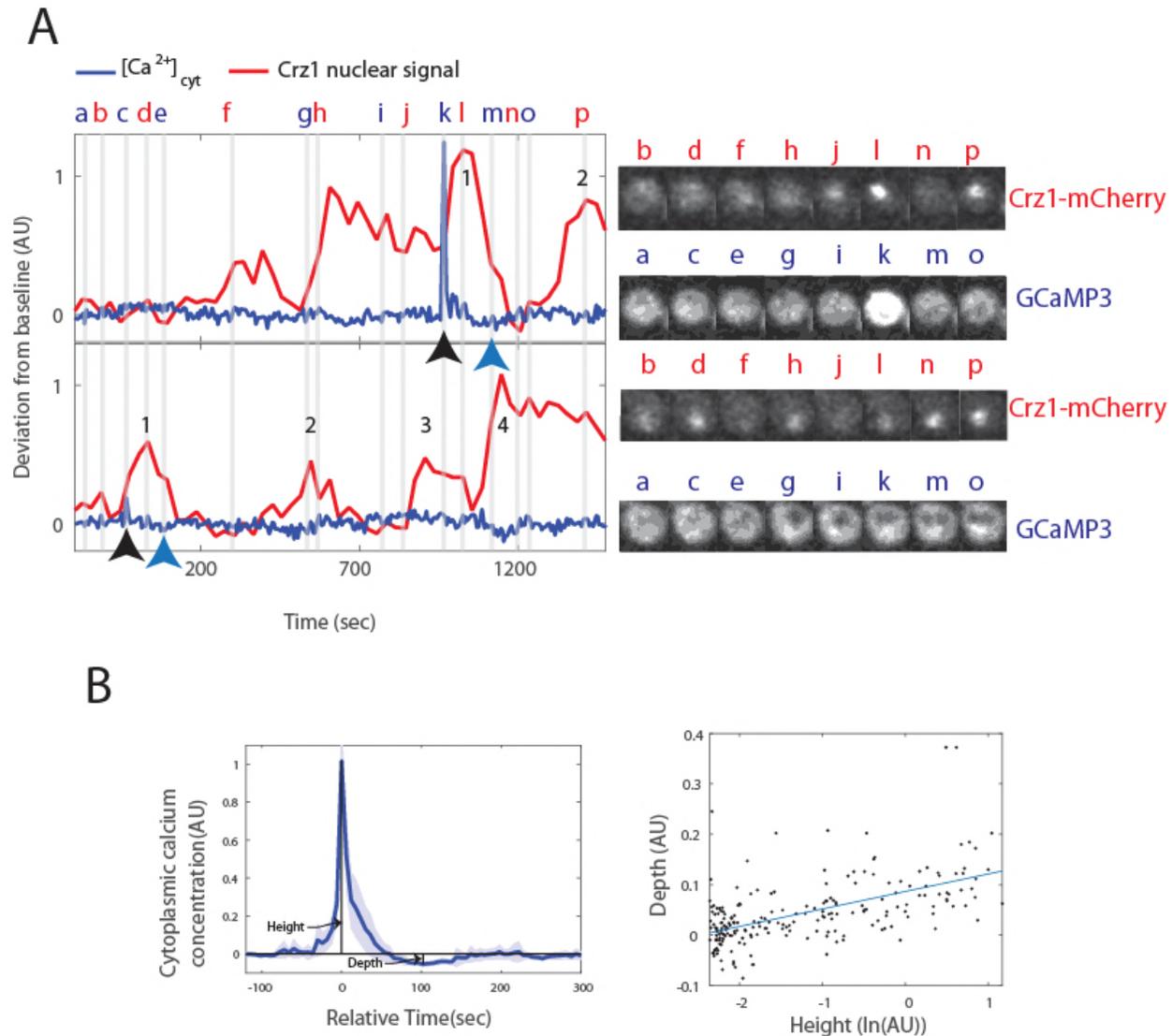
501

502   Figure 1. Calcium pulses with overshoots are found in yeast cells under calcium stress. A) Left

503   panel shows examples of single cell trajectories for Crz1 (red trace) and calcium (blue trace) and

504   snapshots at representative time points from two cells close to each other in the original field of

505   view. Numbers along the red trace indicate the Crz1 pulses identified following a calcium pulse

506   (black arrow below blue trace). Blue arrow indicates the local minimum (so-called overshoot)

507   following the calcium pulse. Images in the right panel show the mCherry channel and GCaMP3

508   channel at points indicated in the left panel. B) Left panel shows the average trace of 50 calcium

509   pulses. Shaded area shows 95% CI of the average trace. Maxima of calcium pulses are aligned to

510   time = 0 sec (Relative time). An overshoot can be found around time = 100 sec. In the right

511   panel, each dot represents a single calcium pulse. The x-axis is in natural log of peak height,

512   while the y-axis is the depth of the overshoot. Blue line shows a linear fit ($R^2 = 0.37$).

513

514
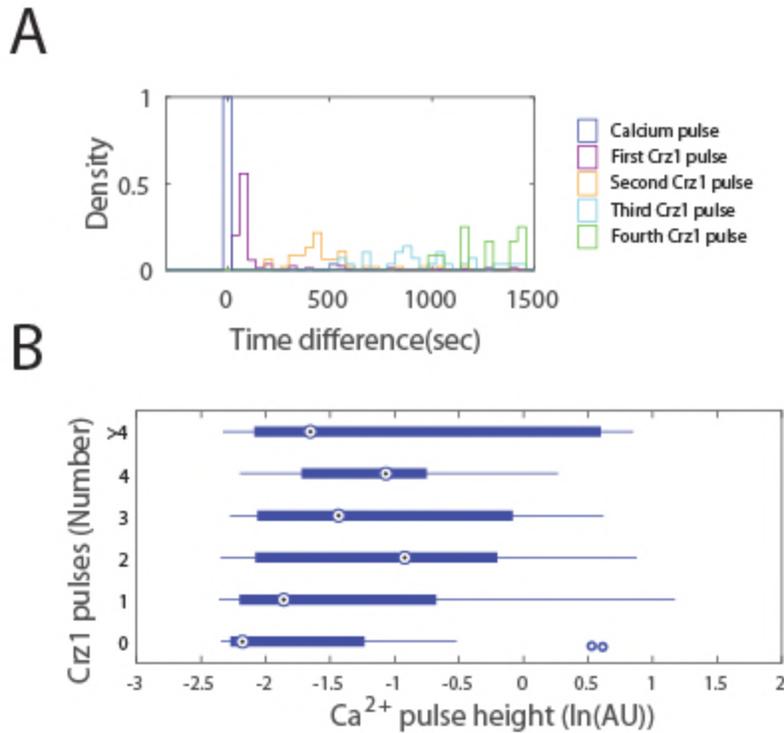
Figure 2. A calcium pulse is followed by multiple Crz1 pulses, and the number of Crz1 pulses is positively correlated to the height of the calcium pulse. A) The density of first, second third and fourth Crz1 pulses (purple, yellow, cyan and green, respectively) is plotted as a function of the time they occur after the calcium pulse (blue). B) Sample sizes of each number of Crz1 pulses are 29 for 0, 73 for 1, 43 for 2, 21 for 3, 16 for >3. Blue boxes indicate the 25% - 75% range, large circles represent the mean, lines represent the range of the data, and individual points show the locations of two outliers.

522

523
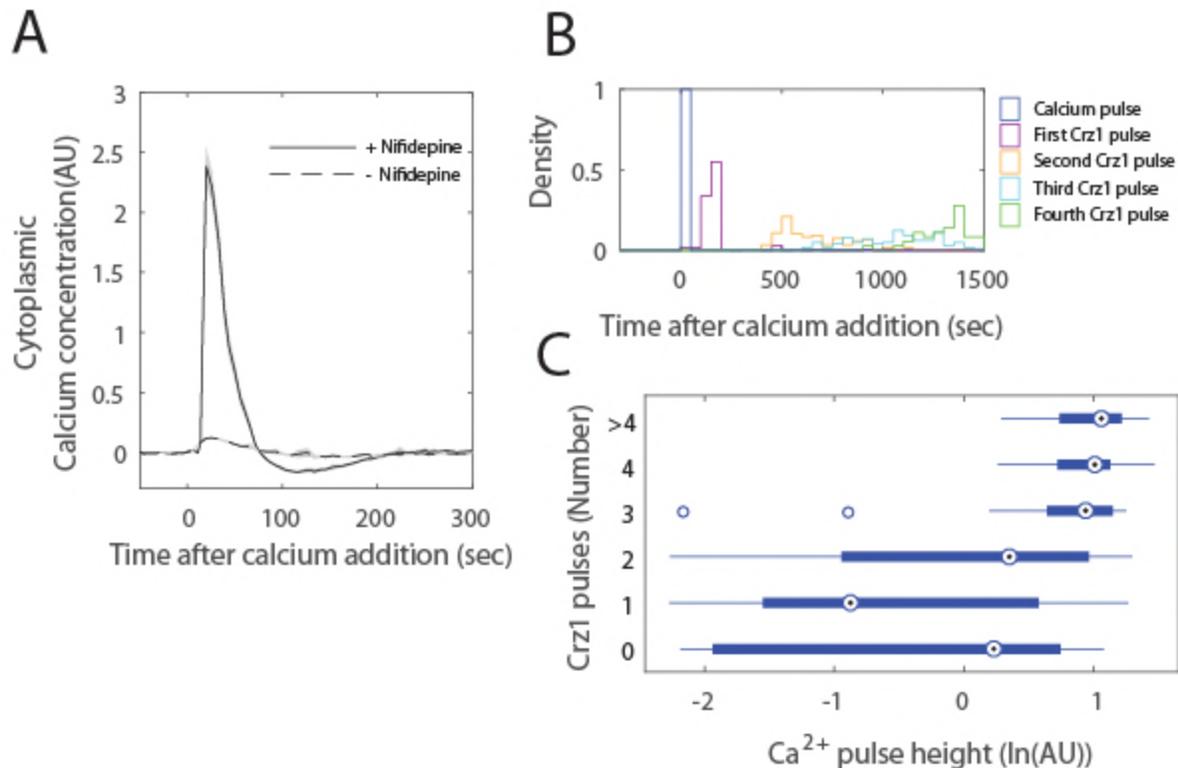
Figure 3. Artificially induced calcium pulses with large average height are followed by more Crz1 pulses. A) Average single cell trajectory (without aligning the maxima) after calcium addition shows synchronized calcium pulses in cells treated with nifedipine (solid line is mean GCaMP3 signal), not in untreated cells (broken line is the mean GCaMP3 from untreated cells. Shaded areas show the 95% CI of mean. B) The density of first, second third and fourth Crz1 pulses (purple, yellow, cyan and green, respectively) is plotted as a function of the time they occur after the calcium pulse (blue). C) Sample sizes of each number of Crz1 pulses are 16 for 0, 36 for 1, 36 for 2, 30 for 3, 48 for 4, 14 for >4. Blue boxes indicate the 25% - 75% range, large circles represent the mean, lines represent the range of the data, and individual points show the locations of outliers.

25

534
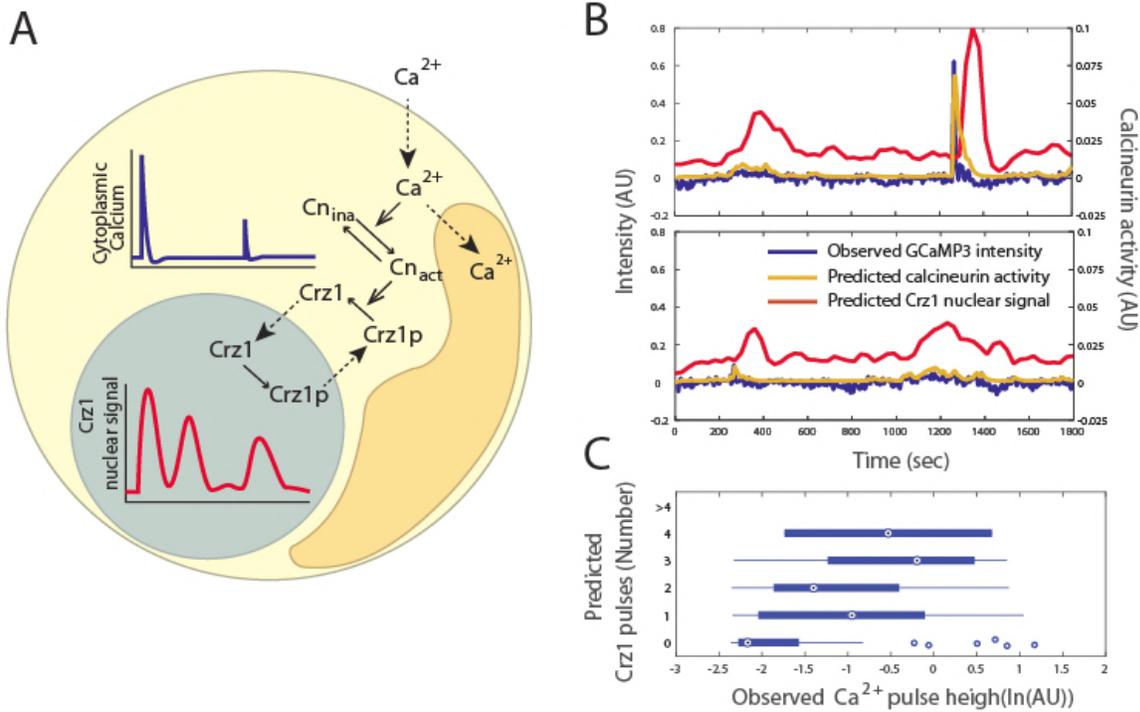
Figure 4. A time delay model for Crz1 nuclear pulsing can qualitatively reproduce Crz1 dynamics after calcium pulses. A) In this single cell model, Ca^{2+} in the cytoplasm (yellow shaded area) is controlled through a two-channel system (dotted arrows crossing from outside the cell to inside, and crossing from yellow shaded area to orange shaded area representing the vacuole). Calcineurin is activated (Cn_{ina} to Cn_{act}) by cytoplasmic calcium, and leads to Crz1 dephosphorylation (Crz1p to Crz1). Dephosphorylated Crz1 is imported (dotted arrow) from cytoplasm (yellow shaded area) to nucleus (grey shaded area) and phosphorylated Crz1 is exported (dotted arrow from nucleus to cytoplasm). B) The Crz1 pulses produced by the model (red trace) following calcium pulses (blue trace). Gold trace shows the calcineurin activity predicted by the model. C) Blue boxes indicate the 25% - 75% range, large circles represent the mean, lines represent the range of the data, and individual points show the locations of outliers. Sample sizes of each number of Crz1 pulses are 68 for 0, 72 for 1, 31 for 2, 9 for 3, 2 for 4, 0 for >4.

26
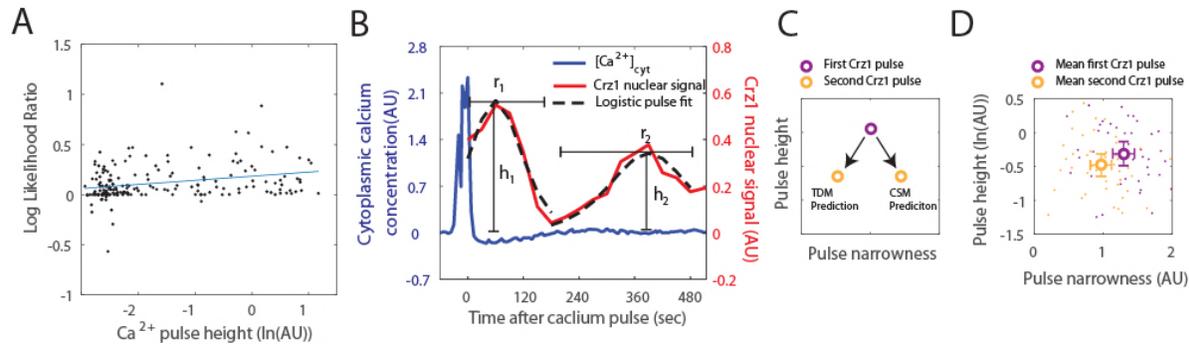
548

549 Figure 5. Predictions of the time delay model are confirmed by experimental data. A) Log

550 likelihood ratio between a periodic and an aperiodic Gaussian process model shows an

551 increasing preference towards the periodic process when calcium pulse height increases (blue

552 line shows a linear fit, $R^2 = 0.07$). Each dot represents the Crs1 trajectory following a calcium

553 pulse. B) shows an example of logistic pulse fit (dotted trace) to experimental data (red trace) for

554 estimating the narrowness (r_1 and r_2) and the heights (h_1 and h_2) of the first and second Crz1

555 pulses after a calcium pulse. C) Conformational switch model (CSM) predicts that the second

556 Crz1 pulse is shorter and narrower than the first Crz1 pulse, while the time delay model (TDM)

557 predicts that the second Crz1 pulse is shorter and less narrow than the first. D) Unfilled circles

558 indicate the mean height and narrowness of Crz1 pulses. The first and second Crz1 pulses are

559 purple and yellow, respectively. Each dot corresponds to a single Crz1 pulse identified following

560 a calcium pulse.

27